

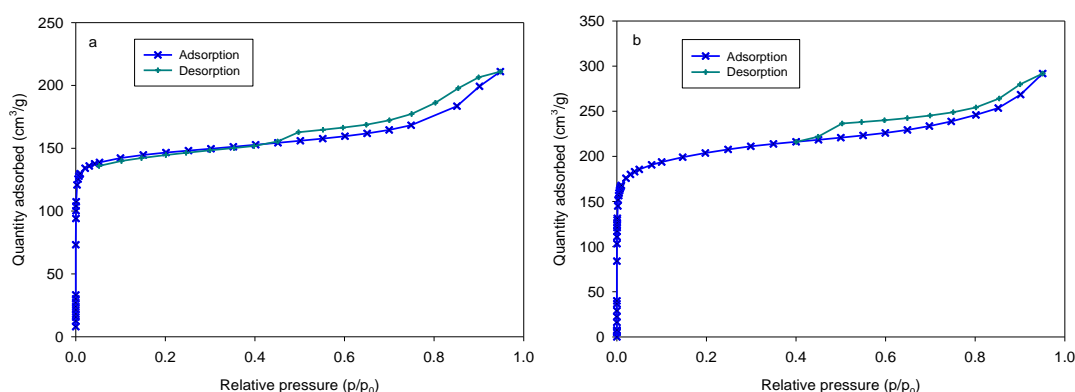
## Supplementary Materials

### Characterization of the different oils obtained through the catalytic in-situ pyrolysis of polyethylene film from municipal solid waste

Lucía Quesada, Mónica Calero, M<sup>a</sup> Ángeles Martín-Lara, Antonio Pérez, Marco F. Paucar-Sánchez, Gabriel Blázquez

#### 3.1. Characterization of the catalysts

Figure S1 shows the N<sub>2</sub> adsorption-desorption isotherms for the three used zeolites. According to IUPAC classification, microporous materials having small external surfaces lead to Type I isotherms; nonporous or macroporous adsorbents yield Type II isotherms; Type III and Type V isotherms represent cases in which there is no identifiable multilayer formation, meaning that there are relatively weak adsorbent-adsorbate interactions; Type IV isotherms are given by mesoporous materials (with pores of 2–50 nm); and Type VI isotherms represent layer-by-layer adsorption on a highly uniform nonporous surface. According to Figure S1, the N<sub>2</sub> isotherms of the three studied zeolites can be classified as type IV isotherms with a well-defined plateau at medium relative pressures and an increase at high relative pressures. Since type IV isotherms are given by the three zeolites, mesoporous channels are presented in these materials [28]. For HY and HUSY zeolites the initial stage of the isotherms sharply rises and then, the isotherm is concave to the P/P<sub>0</sub> axis and the amount adsorbed is lower. The more pronounced uptake at low P/P<sub>0</sub> is associated with the filling of micropores. However, for Ammonium Beta zeolite, the pronounced uptake at low P/P<sub>0</sub> is also observed but, at high P/P<sub>0</sub>, with increasing the P/P<sub>0</sub>, the zeolite shows a higher adsorption amount (Figure S1c). The differences in the shapes of hysteresis loops indicated also differences in the pore structure and adsorption mechanisms. For example, the value of P/P<sub>0</sub> in which the hysteresis loop starts shows some differences among HY, HUSY and Beta zeolite. In addition, hysteresis loops more similar to type H4 loops can be observed for HY and HUSY zeolites and hysteresis loop of type H3 for Beta zeolite. H4 loops are often found with aggregated crystals of zeolites, some mesoporous zeolites, and micro-mesoporous carbons and loops of type H3 are more frequently given by non-rigid aggregates of plate-like particles.



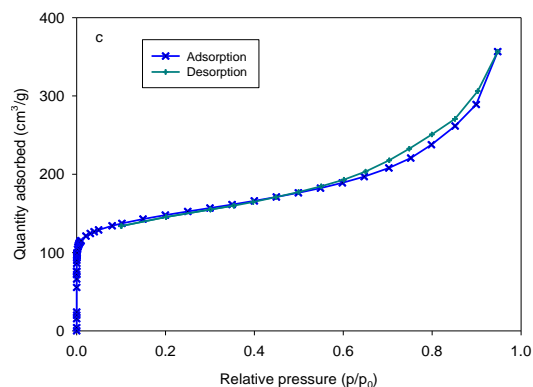


**Figure S1.** N<sub>2</sub> adsorption-desorption isotherms at 77 K of: (a) HY CBV 600 zeolite; (b) HUSY CBV 720 zeolite; (c) Ammonium Beta CP 814E zeolite.

XRD patterns of HY and HUSY samples are shown in Figure S2a. Both zeolites were purely crystalline with the typical diffraction pattern of FAU (faujasite) framework (Structural information on all the Zeolite can be consulted at <http://www.iza-structure.org/databases/>). These are characterized by peaks at 6, 10, 12, 15 and 18° 2 $\theta$ . The FAU structures, sodalities cages are put in the same way as the carbon atoms in diamond and are joined to one another via double 6-rings. This results in what is known as supercages of 1.4 nm at the intersection of the channels and a three-dimensional channel with an equivalent minimum pore size of 0.74 nm [33].

Figure S2b shows the XRD pattern of Ammonium Beta CP 814E EA zeolite. It was purely crystalline with the typical diffraction pattern of the BEA framework. This is characterized by two main peaks at around 7.6 and 22.4° 2 $\theta$ . This zeolite is made up of two cross-linked polymorphs (A and B) stacked almost randomly, generating straight 3D channels with an equivalent minimum pore size of 0.66 × 0.67 nm [33]. This structure gives rise to a significant number of terminal silanol groups. The large diffraction peaks are the result of stacking failures generated by the presence of the two isomorphs [32].

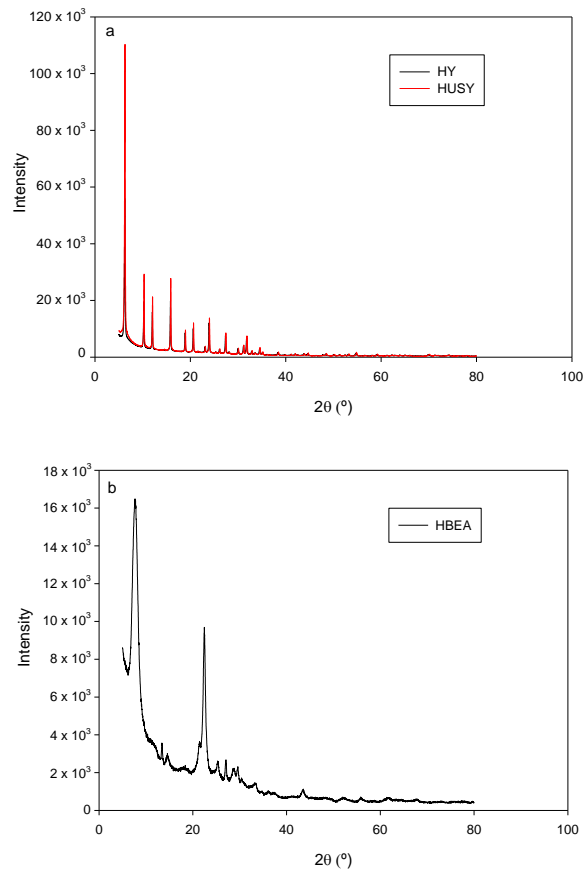
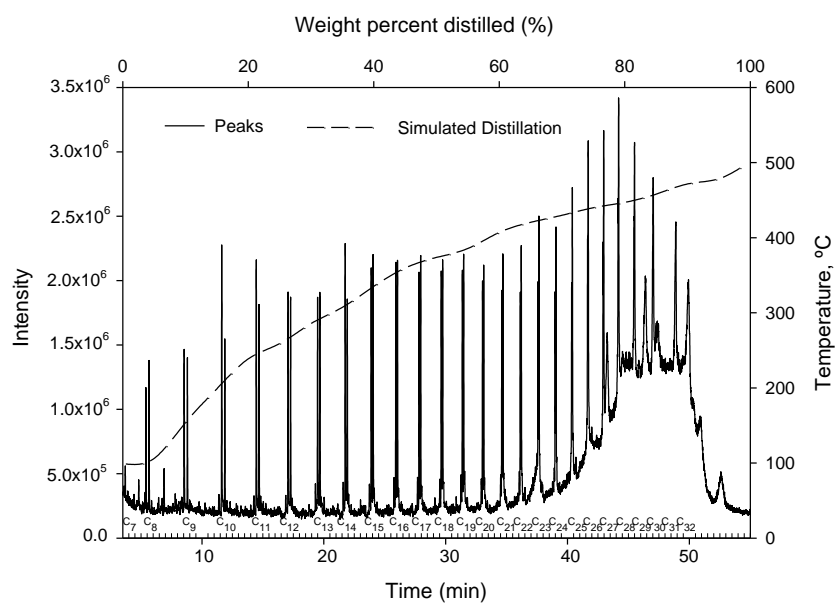
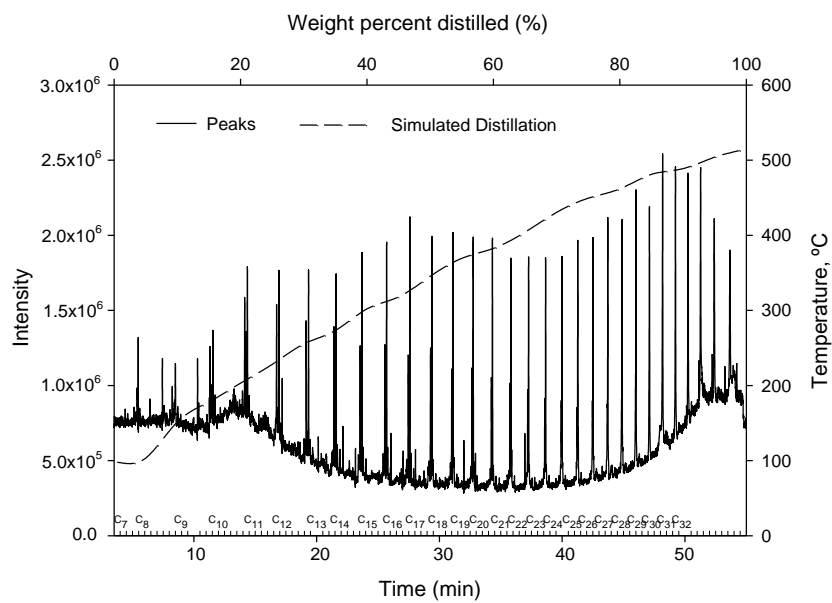


Figure S2. Ray-X pattern of: (a) HY CBV 600 and HUSY CBV 720 zeolite; (b) HBEA CP 814E

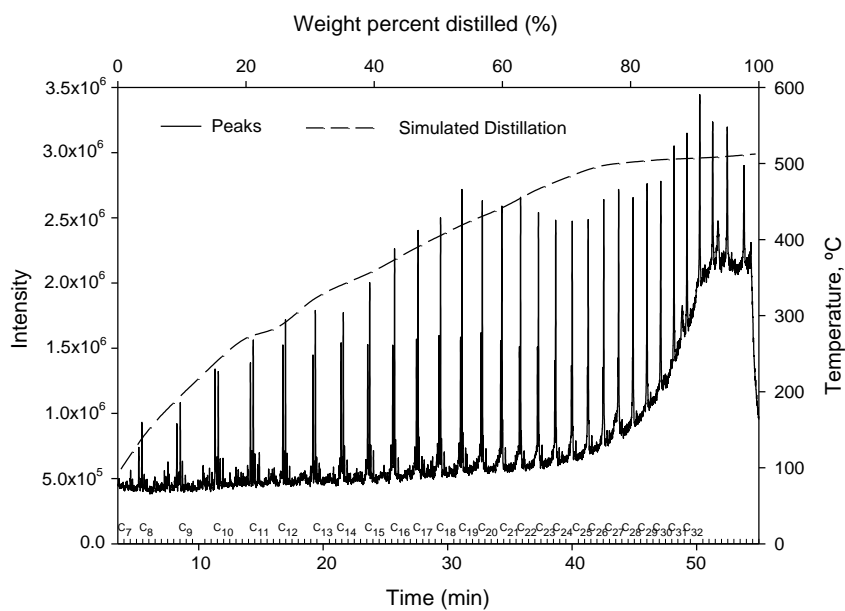
### 3.3.3. GC-MS



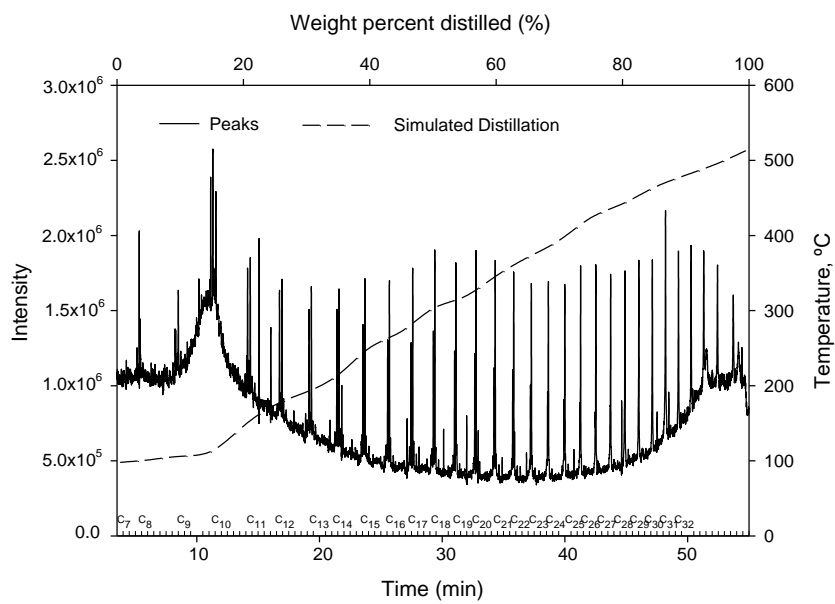
(a)



(b)



(c)



d)

**Figure S3** GC-MS chromatogram and simulated distillation curve of the pyrolytic oil samples from non-catalytic and in-situ pyrolysis: a) without catalyst; b) HY; c) HUSY; d) HBEA

**Table S1** Summary of the hydrocarbon types of pyrolytic oil samples from non-catalytic and in-situ pyrolysis according designations ASTM D2425, D2786, D2789 and ASTM D3239

Hydrocarbons	Hydrocarbon Type	Without catalyst, %Wt	HY, %Wt	HUSY, %Wt	HBEA, %Wt
Paraffins	Paraffins	32.38	28.82	30.36	25.18
Naphtha	Monocycloparaffins	25.66	17.45	19.04	16.79
	Dicycloparaffins	10.80	7.89	13.08	8.11
	Tricycloparaffins	1.11	0.82	12.79	1.15
	Tetracycloparaffins	0.44	0.23	0.40	0.28
	Pentacycloparaffins	1.39	0.69	0.92	0.91
	Hexacycloparaffins	1.09	0.49	0.93	0.67
Aromatics	Monoaromatic	0.36	0.32	0.05	0.33
	Alkyl benzenes	1.65	2.76	2.88	2.14
	Indans or tetralins, or both	0.52	1.42	3.29	2.67
	Indenes or $C_nH_{2n-10}$ , or both	1.12	1.02	1.70	2.43
	Naphthalene	0.68	0.79	0.86	2.29
	Naphthalenes	2.24	0.95	1.05	1.10
	Acenaphthenes or $C_nH_{2n-14}$ , or both	1.03	1.02	1.35	1.07
	Acenaphthylenes or $C_nH_{2n-16}$ , or both	1.59	1.64	2.42	2.42
Tricyclic aromatics	0.25	0.79	2.27	0.82	
Others	Olefins and others	17.69	32.90	6.61	31.65

## References

28. Thommes, M.; Kaneko, K.; Neimark, A.V.; Olivier, J.P.; Rodriguez-Reinoso, F.; Rouquerol, J.; Sing, K.S.W. Physisorption of gases, with special reference to the evaluation of surface area and pore size distribution (IUPAC Technical Report). *Pure Appl. Chem.* **2015**, *87*, 1051–1069.
32. Simon-Masseron, A.; Marques, J.P.; Lopes, J.M.; Ribeiro, F.R.; Gener, I.; Guisnet, M. Influence of the Si/Al ratio and crystal size on the acidity and activity of HBEA zeolites. *Appl. Catal. A-Gen.* **2007**, *316*, 75–82.
33. Baerlocher, Ch.; McCusker, L.B.; Olson, D.H. *Atlas of Zeolite Framework Types*, 6th ed; Elsevier: Amsterdam, the Netherlands, 2007.